

# Transport and Adsorption of Silica Nanoparticles in Carbonate Reservoirs: A Sand Column Study

Qi Liu,<sup>1</sup> Zhonghao Sun,<sup>2\*</sup> and J. Carlos Santamarina

Earth Science and Engineering, King Abdullah University of Science and Technology (KAUST), Thuwal 23955-6900, Saudi Arabia

## S Supporting Information

**ABSTRACT:** The adsorption of nanoparticles onto mineral surfaces is a major limitation for applications that require long transport distances, such as enhanced oil recovery. This study investigates silica nanoparticle transport and adsorption in long granular columns, with emphasis on the adsorption onto carbonate substrates, given the fact that carbonate reservoirs host more than 60% of the world's recoverable oil. The grain-scale particle–mineral interactions are characterized by zeta potential measurements. Ionic strength (especially potential-determining ions:  $\text{Ca}^{2+}$ ,  $\text{Mg}^{2+}$ ,  $\text{CO}_3^{2-}$ , etc.) inherently influences the zeta potential of carbonates. Derjaguin–Landau–Verwey–Overbeek analyses show that low surface potential and high ionic concentration inhibit the electrostatic double-layer repulsion and lower the energy barrier of adsorption. Adsorption column experiments simulate a variety of fluid chemistry conditions: pH, ionic concentration, and ion type. Alkaline and low-salinity conditions favor silica nanoparticles transport in carbonate reservoirs. Both scanning electron microscopy images and adsorption mass analyses suggest that the adsorption of nanoparticles onto carbonate substrates is multilayered. A two-term adsorption model adequately captures the instantaneous adsorption and the subsequent kinetic adsorption. The instantaneous adsorption constant delays particle transport, and the kinetic adsorption rate determines the concentration profile of nanoparticles along the reservoir at the steady state. High advection velocity and low adsorption rate  $k_1$  are required to deliver high nanoparticle concentration to the far field in the reservoir.

## INTRODUCTION

Engineered nanoparticles can augment environmental remediation and enhance oil recovery. In fact, previous studies have shown that nanoparticles selectively capture pollutants (groundwater and wastewater treatment<sup>1–4</sup>), alter wettability,<sup>5–7</sup> reduce interfacial tension,<sup>8,9</sup> enhance spreading,<sup>10–12</sup> and alter the rheological properties of suspensions.<sup>13,14</sup>

The retention of nanoparticles onto mineral surfaces is a major limitation for applications that require long transport distances, such as oil recovery.<sup>15–17</sup> In addition, although small size nanoparticles (10–100 nm) can easily fit through micron-size pore throats,<sup>18</sup> particle aggregation in unstable nanofluids favors particle straining and clogging and aggravates transport difficulties.<sup>8,19</sup>

Previous studies have investigated the transport and retention of different types of nanoparticles in porous media, such as metal oxide nanoparticles,<sup>20,21</sup> metallic nanoparticles,<sup>22,23</sup> carbon nanotubes,<sup>24</sup> fullerol,<sup>25</sup> and silica nanoparticles.<sup>26,27</sup> In most cases, porous media are made of either glass beads or quartz sand.<sup>28,29</sup> Results show no significant flow rate effects for silica nanoparticles.<sup>25</sup> On the other hand, the mineral composition and solution chemistry (i.e., pH, ionic strength, and type of cations) can readily alter nanoparticle transport.<sup>21,23,28</sup> Clay content in natural sediments is also an important factor for nanoparticle transport.<sup>30</sup>

Carbonate reservoirs host more than 60% of the world's recoverable oil and 40% of the world's gas.<sup>31</sup> There are only a few studies on nanoparticle transport in carbonate reservoirs;<sup>28</sup> some laboratory core flooding tests show a 10% increase in enhanced oil recovery following the injection of nanofluids.<sup>32–36</sup> Once again, particle transport emerges as the

limiting factor. Adsorption experiments with silica nanoparticles on calcite substrates highlight strong fluid chemistry effects, in particular, lower pH, and higher ionic strength enhances adsorption.<sup>37</sup> Furthermore, core flooding tests show higher adsorption of silica nanoparticles (with 2% NaCl) in limestone and dolomite than in sandstone.<sup>26</sup>

This study aims to advance our understanding of nanoparticle transport and adsorption in carbonate reservoirs. We present a comprehensive study including the characterization of grain-scale interactions, the measurement of nanoparticle transport in adsorption columns as a function of fluid chemistry (pH, ionic concentration, and ion type), and both grain-scale and macroscale analyses to gain physical insight into underlying adsorption and transport processes. The following section describes the tested materials and characterization protocols.

## EXPERIMENTAL STUDY: MATERIALS AND PROCEDURES

**Materials.** Experiments use 10 nm silica nanoparticles (Sigma-Aldrich). The average aggregate size in dispersion is  $74 \pm 18$  nm (dynamic light-scattering method—Zetasizer ZS). We prepare all nanofluids with a mass concentration of  $C_0 = 2$  g/L in agreement with potential engineering applications such as enhanced oil recovery and sonicate suspensions for 40 min to break weak bonds between particles and enhance dispersion (Fisher Scientific Model 505 Sonic Dismembrator). We adjust the pH with either HCl or NaOH.

Received: January 10, 2019

Revised: March 27, 2019

Published: April 25, 2019

The porous medium is made of carbonate sand. The crushed Jeddah sand contains 47% calcite and 53% dolomite, the particle size ranges between 0.25 and 0.43 mm, and the specific surface is 36.2  $\text{cm}^2/\text{g}$ . For comparison, we also run tests on a packing of uniform silica sand to simulate a siliceous reservoir.

**Zeta Potential Measurements.** The zeta potential provides quantitative information needed for the analysis of suspension stability (particle–particle interaction) and adsorption (particle–surface interaction). We use electrophoretic mobility to determine the zeta potential of the silica nanoparticles and carbonate powder crushed to  $d < 50 \mu\text{m}$  (Zetasizer Nano ZS, Malvern Instruments).

**Adsorption Column Experiments.** Figure 1 shows a sketch of the adsorption column (length  $L = 150 \text{ cm}$ , inner diameter of 6.35

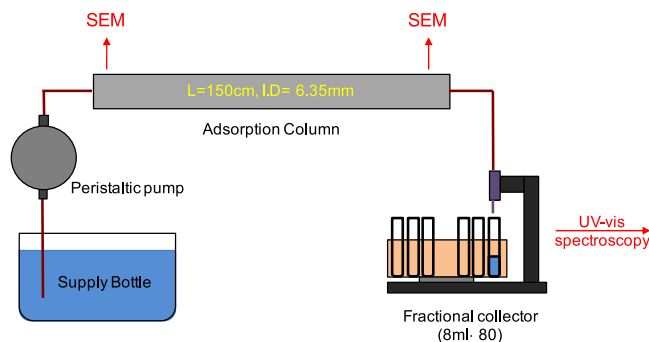


Figure 1. Adsorption column—components.

mm), the peristaltic pump at the inlet (constant flow rate of 1 mL/min), and the fraction collector at the outlet (model 2110, Bio-Rad). The pore volume in the sand-filled adsorption column is 18  $\text{cm}^3$ . We use UV–vis spectroscopy (Cary 500 UV–vis–NIR spectrophotometer, Agilent Technologies) to determine the concentration of nanoparticles in each test tube in the effluent collector. Calibration tests show a linear relationship between absorbance at a wavelength of 212 nm and nanoparticle concentration  $C$  [g/L].

All column experiments follow the same test protocol: (1) inject 90 mL of the test solution without nanoparticles to condition the sand column, (2) inject 90 mL of the nanofluid, and (3) inject 90 mL of the test solution without nanoparticles to flush the sand column. Finally, we collect sand samples from the inlet and the outlet, dry them in an oven (105  $^\circ\text{C}$ , overnight), and image them using scanning electron microscopy (SEM) (Quanta 600 FEG).

## RESULTS

We report first experimental results for the surface charging characteristics of silica particles and carbonate powders, followed by the measurements gathered in adsorption column experiments.

**Zeta Potential of Silica and Carbonate.** A diffused counterion cloud forms around a charged particle submerged in water. The zeta potential  $\zeta$  at the shear plane provides critical information needed to analyze the electrostatic interactions between particles, suspension stability, and adsorption of particles on mineral substrates.

Figure 2a shows the zeta potential of silica nanoparticles as a function of pH. The silica nanoparticles have a high negative charge in alkaline conditions and become slightly positively charged as  $\text{pH} \leq 4$ .

Figure 2b,c present the effect of ionic concentration on the zeta potential of silica nanoparticles and carbonate powder. The concentration of NaCl has a negligible effect on the zeta potential of both substrate materials until its concentration exceeds 0.01 M; then, the zeta potential reduces toward 0 mV as the ionic concentration approaches 1 M (Figure 2b). In the

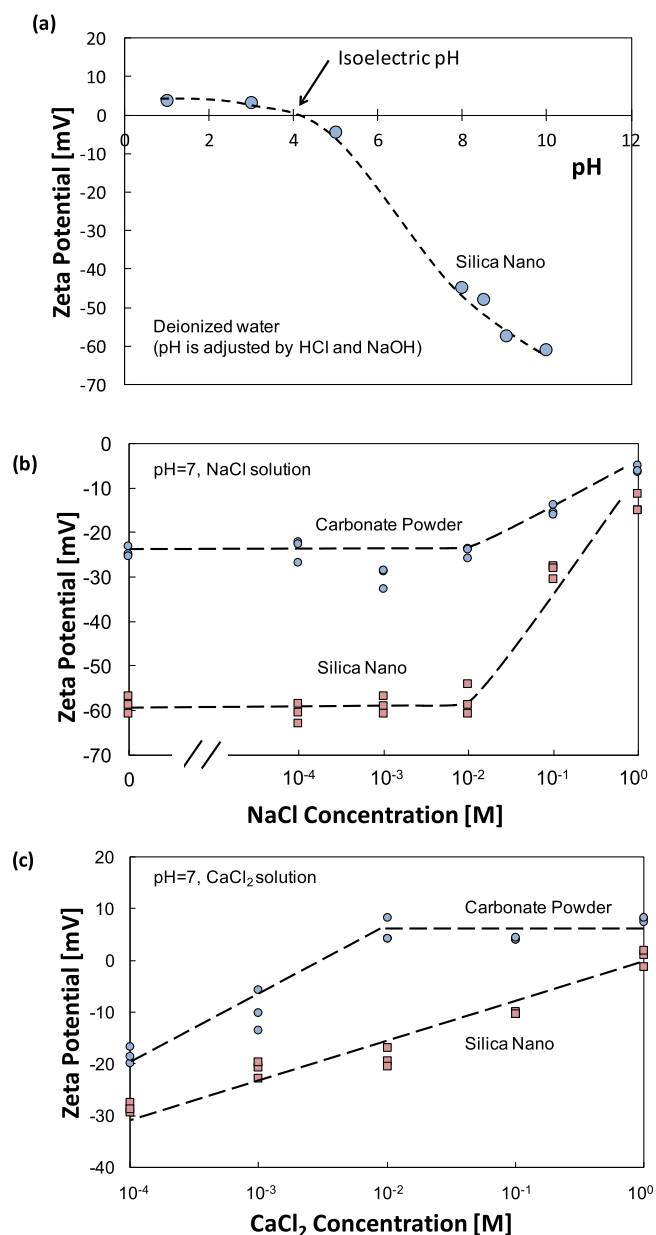
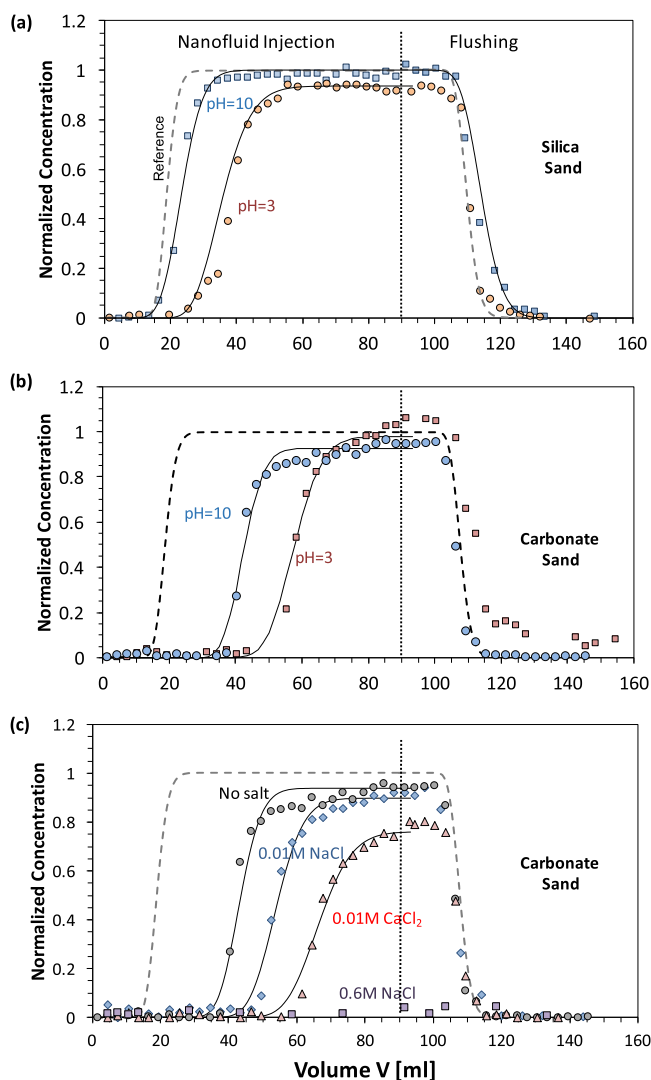


Figure 2. Zeta potential of silica and carbonate. (a) Effect of pH: silica nanoparticles. (b) Effect of NaCl concentration: silica nanoparticles and carbonate powder. (c) Effect of  $\text{CaCl}_2$  concentration: silica nanoparticles and carbonate powder.

presence of divalent  $\text{Ca}^{2+}$ , the zeta potential of carbonate powder and silica nanoparticles changes at low concentration ( $c = 10^{-4} \text{ M}$ ) and becomes positive when  $c = 1 \text{ M}$  for silica and  $c = 0.01 \text{ M}$  for carbonate (Figure 2c).

**Adsorption Column Experiments.** Figure 3 shows the breakthrough curves in terms of the effluent concentration normalized by the influent concentration versus the injection volume  $V$ . The reference signature shown as a dashed line corresponds to the injection of 0.5 M NaCl solution without nanoparticles into the adsorption column saturated with deionized water; this data set provides a reference curve for advection–dispersion transport without adsorption and allows us to compute the dispersion coefficient  $D$  for solutions in these porous media.

**Silica Sand.** Figure 3a shows the results of a limited study conducted with the column filled with silica sand; although



**Figure 3.** Breakthrough curves for adsorption column tests. Dashed lines are reference curves and solid lines are model fittings. (a) Breakthrough curves for nanoparticle injections with pH = 3 and pH = 10 solution in silica porous media. (b) Breakthrough curves for nanoparticle injections with pH = 3 and pH = 10 solution in carbonate porous media. (c) Breakthrough curves for nanoparticle injections with pH = 10 solution in carbonate porous media. Ionic conditions of nanofluids are no salt, 0.01 M NaCl, 0.01 M CaCl<sub>2</sub>, and 0.6 M NaCl.

these tests were run for comparison only, results are relevant to siliceous reservoirs. Breakthrough curves correspond to nanofluids prepared at pH = 3 and pH = 10. The mass of nanoparticles transported through the adsorption column is the integral of breakthrough curves: the nanofluid prepared at pH = 10 exhibits limited adsorption (2% of the input mass), whereas the nanofluid at pH = 3 experiences severe adsorption (17% of the input mass). The limited absorption of nanoparticles at pH = 10 is reversible and large amounts of nanoparticles are recovered after flushing with pH = 10 solution without nanoparticles. This is not the case in the pH = 3 test where only a minor amount of nanoparticles is released during flushing a clean pH = 3 solution. SEM images after the pH = 3 test show nanoparticles coating the silica sand surfaces (Figure 4).

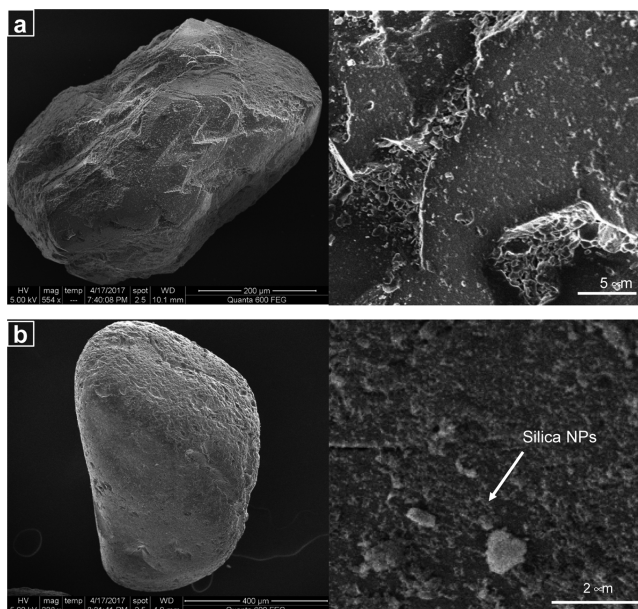


**Figure 4.** SEM images of silica sand grains. (a) Clean silica sand grain. (b) Silica sand after pH = 3 nanofluid injection and flushing. See high-resolution images in Supporting Information S3.

**Carbonate Sand.** Figure 3b shows the breakthrough curves for nanoparticle transport through carbonate porous media at pH = 3 and pH = 10. Calcite and dolomite dissolution at pH = 3 releases Ca<sup>2+</sup> and Mg<sup>2+</sup> into the aqueous solution, the pH reaches pH = 7.6 at the outlet, and there is more severe adsorption of nanoparticles compared to that during the test at pH = 10 solution. The insoluble minerals released during the test at pH = 3 may explain the high normalized nanoparticle concentration  $C/C_0 > 1$  during the early stages of flushing.

Figure 3c presents the breakthrough curves for nanofluid injections through carbonate sand where the salt concentration in injected nanofluids is no salt, 0.01 M CaCl<sub>2</sub>, 0.01 M NaCl, and 0.6 M NaCl. The addition of salts to nanofluids enhances the adsorption of nanoparticles. Bivalent CaCl<sub>2</sub> causes more adsorption compared with monovalent NaCl at the same salt concentration 0.01 M. There is no nanoparticle breakthrough in the experiment with the 0.6 M NaCl nanofluid, indicating that all nanoparticles remained adsorbed in the carbonate porous medium (Figure 3c).

SEM images of carbonate sand grains recovered from the inlet and the outlet after nanofluid injections suggest monolayer adsorption for nanofluids with no salt and a multilayer adsorption for nanofluids with 0.01 M CaCl<sub>2</sub> and 0.6 M NaCl (Figure 5). Carbonate sand grains recovered near the outlet after the injection of the 0.6 M NaCl nanofluid are clean; this confirms that all nanoparticles are adsorbed along the column before reaching the outlet.

## ANALYSES AND DISCUSSION

Experimental results highlight the differences in silica and carbonate electrostatic interactions as a function of pH and ionic strength, ensuing implications on nanoparticle adsorption.

**Silica and Carbonate Surface Charge.** Protons H<sup>+</sup> and hydroxyl OH<sup>-</sup> neutralize free bonds in SiO<sub>4</sub><sup>4-</sup> tetrahedrons on silica particles to form silanol groups [Si(OH)<sub>n</sub>]. Therefore, H<sup>+</sup> and OH<sup>-</sup> behave as potential-determining ions,<sup>38,39</sup> and the

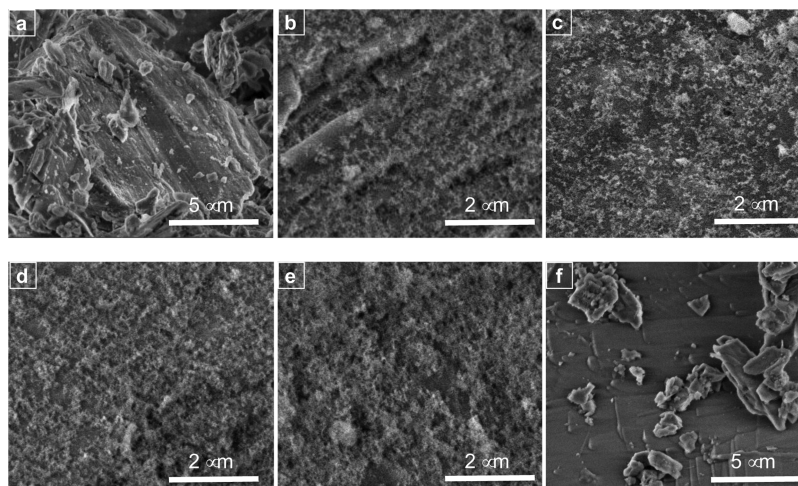


**Figure 5.** SEM images of carbonate sand grains after nanofluid injection and flushing. (a) Clean carbonate. (b) From outlet pH = 3. (c) From outlet pH = 10. (d) From outlet pH = 10 and  $c(\text{CaCl}_2) = 0.01$  M. (e) From inlet pH = 10 and  $c(\text{NaCl}) = 0.6$  M. (f) From outlet pH = 10 and  $c(\text{NaCl}) = 0.6$  M. High-resolution images are available in [Supporting Information S3](#).

surface charge of silica particles is a function of the fluid pH (Figure 2a). Differences between the response to  $\text{Na}^+$  and  $\text{Ca}^{2+}$  ions agree with the binding affinities of alkali cations on silica surfaces:  $\text{Ca}^{2+} > \text{Mg}^{2+} \gg \text{K}^+ > \text{NH}_4^+ > \text{Na}^+ > \text{Li}^+$ .<sup>39,40</sup>

Calcite dissolution releases lattice ions  $\text{Ca}^{2+}$  and  $\text{CO}_3^{2-}$ , which are potential-determining ions in carbonates. Experimental results show that  $\text{Ca}^{2+}$  concentration has a pronounced influence on the zeta potential of carbonates (Figure 2c). Although pH determines the equilibrium concentration of  $\text{Ca}^{2+}$  and  $\text{CO}_3^{2-}$  in aqueous solutions, protons  $\text{H}^+$  and hydroxyl  $\text{OH}^-$  themselves are not potential-determining ions for calcite.<sup>41</sup>

**Grain Scale Adsorption Behavior.** Gravitational and drag forces are negligible compared to the electrical interparticle forces that nanoparticles experience.<sup>42</sup> The total particle interaction energy  $U_T$  adds the London–van der Waals interaction energy  $U_{\text{VDW}}$  and the electrostatic double-layer energy  $U_{\text{EDL}}$

$$U_T = U_{\text{VDW}} + U_{\text{EDL}} \quad (1)$$

Sand grains are >1000 times larger than nanoparticles, so we analyze their interaction as a sphere of radius  $R$  at a distance  $a$  from a flat surface. The van der Waals interaction energy is<sup>17,43</sup>

$$U_{\text{VDW}} = -\frac{A_H}{6} \left[ \frac{R}{a} + \frac{R}{a+2R} + \ln\left(\frac{a}{a+2R}\right) \right] \quad (2)$$

where the Hamaker constant  $A_H$  [J] combines the permittivities of the fluid and solids involved. The electrostatic double-layer interaction energy for a sphere next to a flat surface in a 1:1 electrolyte solution with concentration  $c$  [mol] is<sup>43–45</sup>

$$U_{\text{EDL}} = 64\pi R \epsilon_0 \epsilon_r \tanh\left(\frac{e_0 \psi_s}{4kT}\right) \tanh\left(\frac{e_0 \psi_p}{4kT}\right) \left(\frac{kT}{e_0}\right)^2 \exp(-\kappa a) \quad (3)$$

where  $\epsilon_r$  is the relative dielectric permeability [–],  $\psi_s$  is the sphere surface potential [mV],  $\psi_p$  is flat surface potential [mV], and the Debye length  $\kappa^{-1}$  is

$$\kappa^{-1} = \left( \frac{\epsilon_0 \epsilon_r kT}{2N_A e_0^2 c} \right) \quad (4)$$

The universal constants are the Avogadro number  $N_A = 6.02 \times 10^{23}$ , Boltzmann constant  $k = 1.38 \times 10^{-23} \text{ m}^2 \text{ kg} \cdot \text{s}^{-2} \text{ K}^{-1}$ , and the elementary charge  $e_0 = 1.602 \times 10^{-19} \text{ C}$  and  $T$  is temperature [K].

Let us use the measured zeta potentials instead of surface potentials to calculate electrostatic interactions and accept that the interparticle distance is measured from the shear planes. Figure 6 presents the normalized total energy  $U_T/(kT)$  versus the normalized distance  $\kappa a$  for nanoparticle-to-substrate interaction computed using eqs 1–3. The energy barrier for adsorption decreases as the ionic concentration increases (Figure 6a) and the zeta potential decreases (Figure 6b).

The pore fluid pH determines the zeta potential of silica. Both silica sand and nanoparticles exhibit a highly negative zeta potential at pH = 10 and  $\zeta_{\text{silica}} = -62$  mV, and strong electrostatic repulsion prevents adsorption (Figure 3a). At pH = 3, the zeta potential is low in both silica sand and nanoparticles,  $\zeta_{\text{silica}} = +3$  mV, the energy barrier diminishes (Figure 6b), and some adsorption takes place, which is driven by van der Waals attraction (Figure 3a).

On the other hand, high ionic concentration in the pore fluid lowers the zeta potential of carbonate (Figure 2b,c) and suppresses electrostatic repulsion (Figure 6b), thus promoting adsorption (Figure 3c). The high adsorption and the lack of nanoparticle breakthrough in the experiment with 0.6 M NaCl nanofluid point to shielding of double-layer repulsion and the tendency to aggregation.

Nanoparticle adsorption is more pronounced for the  $\text{CaCl}_2$  solution than the NaCl solution at the same concentration  $c = 0.01$  M because the potential-determining  $\text{Ca}^{2+}$  ion reduces the surface potential of calcite more effectively than  $\text{Na}^+$  (note: the charged carbonate surface has  $\zeta_{\text{carbonate}} = +6$  mV for 0.01 M  $\text{CaCl}_2$  solution, vs  $\zeta_{\text{carbonate}} = -24$  mV for the 0.01 M NaCl solution). The carbonate rock releases  $\text{Ca}^{2+}$  ions when low-pH fluids invade the reservoir; therefore, nanoparticle adsorption is higher for the pH = 3 than for the pH = 10 nanofluid.

Strong adsorption results in multilayer adsorption as confirmed using SEM images (Figure 5). Table 1 summarizes the adsorption data for silica nanoparticles in carbonate sand

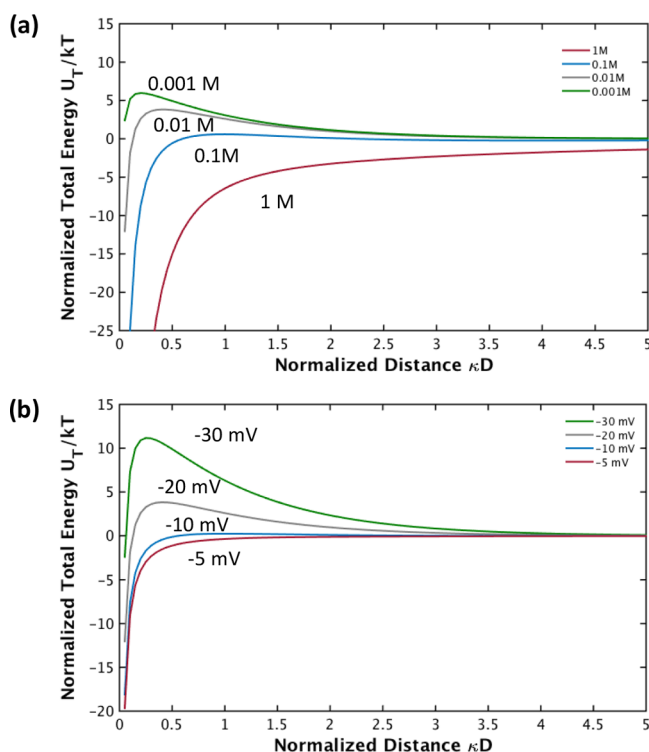


**Figure 6.** Silica particle–surface interaction energy in 1:1 electrolyte solution calculated with DLVO theory. (a) Effect of ionic concentration (constant surface potential:  $-20$  mV). (b) Effect of surface potential (constant ionic concentration:  $0.01$  M).

**Table 1. Mass Analyses for the Adsorption of Silica Nanoparticles in Carbonate Porous Media<sup>a</sup>**

	no salt	0.01 M CaCl <sub>2</sub>	0.01 M NaCl	0.6 M NaCl
injection mass [g]	0.18	0.18	0.18	0.18
collected mass [g]	0.125	0.063	0.094	0
trapped mass [g]	0.055	0.117	0.086	0.18
adsorption proportion [%]	30	65	48	100
total surface area $A_0$ [cm <sup>2</sup> ]	2860	2860	2860	2860
adsorption area <sup>b</sup> $A_{Ad}$ [cm <sup>2</sup> ]	2887	6142	4515	9449
ratio $A_{Ad}/A_0$	1.01	2.15	1.56	3.30

<sup>a</sup>Injection fluid: pH = 10 <sup>b</sup>For monolayer adsorption, the coated adsorption area  $A_{AD}$  is a function of trapped mass  $M_d$ , nanoparticle diameter  $d$ , and density  $\rho$ :  $A_{AD} = 6M_d/(\rho\pi d)$ .

experiments. In fact, the ratio between the adsorption area and the available surface area in the adsorption column  $A_{Ad}/A_0$  is larger than 2 for experiments with 0.01 M CaCl<sub>2</sub> and 0.6 M NaCl.

**Macroscale Transport Model.** Mass balance requires that the variation of particle concentration at a given location  $x$  during nanofluid injection combines the contribution by dispersion, advection and the rate of adsorption (see Supporting Information S2 for the derivation)

$$\frac{\partial C}{\partial t} + \frac{\rho}{e} \frac{\partial S}{\partial t} = D \frac{\partial^2 C}{\partial x^2} - v \frac{\partial C}{\partial x} \quad (5)$$

The variables in this equation are the nanoparticle concentration in the fluid  $C$  [kg/m<sup>3</sup>], the mass of adsorbed

nanoparticles per unit mass of substrates  $S$  [kg of adsorbed particles/kg of grain minerals], the dispersion coefficient  $D$  [m<sup>2</sup>/s], the advection velocity  $v$  [m/s], the mineral density  $\rho$  [kg/m<sup>3</sup>], and the void ratio  $e$  [–].

We adopt a two-term adsorption model  $S = S_1 + S_2$  to capture the concentration-dependent instantaneous adsorption ( $S_2$ ) and subsequent kinetic adsorption ( $S_1$ )

$$\frac{\partial S_1}{\partial t} = \frac{k_1 e}{\rho} C \quad \text{and} \quad S_2 = \frac{K_2 e}{\rho} C \quad (6)$$

with proportionality factors being the adsorption rate  $k_1$  [s<sup>-1</sup>] and the instantaneous adsorption constant  $K_2$  [–]. Therefore, the total adsorption  $S$  is

$$\frac{\partial S}{\partial t} = \frac{e}{\rho} \left( k_1 C + k_2 \frac{\partial C}{\partial t} \right) \quad (7)$$

Finally, the expression for time-varying concentration in advection–dispersion–adsorption transport becomes (modified from ref 46)

$$(1 + K_2) \frac{\partial C}{\partial t} = D \frac{\partial^2 C}{\partial x^2} - v \frac{\partial C}{\partial x} - k_1 C \quad (8)$$

Figure 3a–c shows fitted breakthrough curves using eq 8. The advection velocity  $v$  is known from the imposed injection rate ( $v = 0.138$  cm/s). The dispersion coefficient  $D$  is inferred by matching the breakthrough curve for the 0.5 M NaCl solution without nanoparticles ( $D = 0.14$  cm<sup>2</sup>/s—see Supporting Information S1 for the procedure to determine the dispersion coefficient). The fitted adsorption rate  $k_1$  and the instantaneous constant  $K_2$  for nanofluids are listed in Table 2.

**Table 2. Adsorption Parameters Used in the Model**

mineral	pH	ionic strength	adsorption rate $k_1$ [s <sup>-1</sup> ]	instantaneous adsorption constant $K_2$ [–]
silica	pH = 3	no salt	$6 \times 10^{-5}$	1
	pH = 10		0	0.2
carbonate	pH = 3	no salt	$2 \times 10^{-5}$	2.2
		no salt	$6 \times 10^{-5}$	1.4
	pH = 10	0.01 M NaCl	$1 \times 10^{-4}$	2
		0.01 M CaCl <sub>2</sub>	$2.5 \times 10^{-4}$	2.7

Experimental results and analytical models show both a delay in breakthrough and a change in the plateau concentration as a function of pH and ionic strength. The adsorption rate  $k_1$  increases when multilayer adsorption takes place. Multilayer adsorption relies on particle–particle interaction and will be weaker than particle–mineral adsorption in most cases. On the other hand, the concentration-dependent instantaneous adsorption controls the delay in nanoparticle breakthrough. Decreasing the zeta potential and increasing the ionic strength favor particle-to-mineral adsorption and lead to a higher equilibrium constant  $K_2$ .

**Reservoir Implications.** Experimental results and model-based analyses reported above help analyze the interplay between adsorption, dispersion, and advection during nanoparticle transport through porous media. Clearly, mineralogy,

fluid chemistry, and injection conditions affect the ability to transport nanoparticles over long distances in reservoirs.

Table 3 summarizes the dimensionless ratios that govern the transport–adsorption behavior of nanoparticles at the reservoir

**Table 3. Governing Dimensionless Ratios**

dimensionless ratios	physical meaning
$x/L$	relative position
$C_{x,t}/C_0$	concentration $C_{x,t}$ at position $x$ and time $t$ relative to the input concentration $C_0$
$t_D = vt/L$	time $t$ relative to the duration of advection $L/v$
$B = vL/4D$	role of advection relative to the role of dispersion
$K_1 = k_1L/v$	adsorption rate relative to advection rate
$K_2$	instantaneous adsorption constant

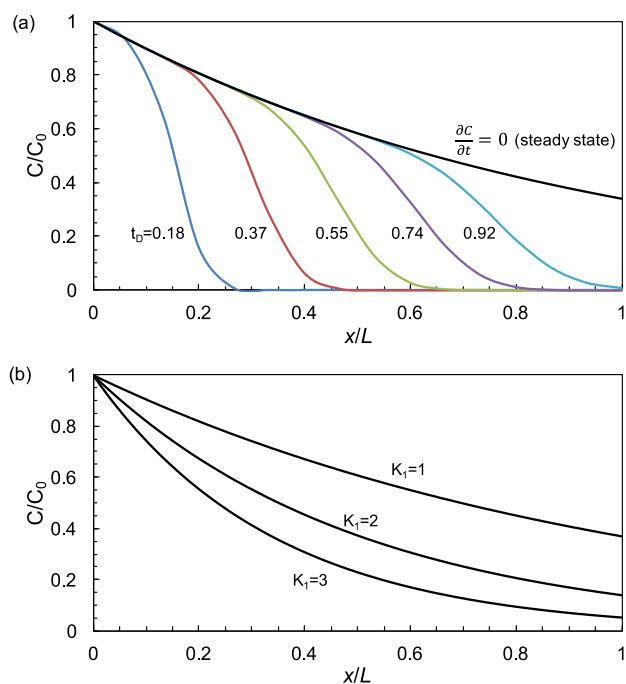


**Figure 7.** Nanoparticle transport vs distance. (a) Evolution of nanoparticle concentration along the reservoir. The concentration profile approaches the steady-state solution as  $t_D$  increases ( $K_1 = 1$ ,  $K_2 = 0.2$ , and  $B = 36$ ). (b) Influence of dimensionless adsorption rate  $K_1$  on the steady-state concentration profiles.  $K_1 = 1, 2$ , and  $3$  ( $B = 36$ ).

scale. The dimensionless solutions plotted in Figure 7a show the evolution of nanoparticle concentration along the reservoir ( $K_1 = 1$ ,  $K_2 = 0.2$ , and  $B = 36$ ). The concentration profile approaches the steady state ( $\partial C/\partial t = 0$ ) as dimensionless time  $t_D$  increases. The steady state is a state of continuous adsorption and applies while pore topology changes remain small.

The instantaneous adsorption delays the transport process. A high instantaneous adsorption constant  $K_2$  requires more nanofluid injection to reach the steady state; however, it does not change the concentration profile in the steady state. On the other hand, Figure 7b shows the influence of the dimensionless adsorption rate  $K_1 = k_1L/v$  on the steady-state concentration profile ( $K_1 = 1, 2$ , and  $3$ ): a higher advection velocity  $v$  and lower adsorption rate  $k_1$  render a small value of  $K_1$ , which

benefits the delivery of high nanoparticle concentration to the far field in the reservoir.

## CONCLUSIONS

We investigated the transport of silica nanoparticles in a long granular column, with emphasis on the adsorption onto carbonate substrates. Notable conclusions from this study are listed below.

- The zeta potential is pH-dependent in silica, but it is controlled by ions such as  $\text{Ca}^{2+}$ ,  $\text{Mg}^{2+}$ , and  $\text{CO}_3^{2-}$  in carbonates. On the other hand, high salt concentration collapses the double layer around silica and carbonate. In combination, lower surface potential and higher ionic concentration inhibit the electrostatic double-layer repulsion and lower the energy barrier of adsorption.
- Breakthrough curves confirm adsorption trends that are consistent with zeta potential measurements and Derjaguin–Landau–Verwey–Overbeek (DLVO) analyses. There is high adsorption of nanoparticles in low-pH solutions in silica sand and high-salinity solutions in carbonate sand. Conversely, alkaline and low-salinity conditions favor silica nanoparticles transport in carbonate reservoirs.
- The adsorption of nanoparticles onto carbonate substrates is multilayered. A two-term adsorption model adequately captures instantaneous adsorption and the subsequent kinetic adsorption.
- High advection velocity and a low adsorption rate are required to deliver a high concentration of nanoparticle to the far field in the reservoir.

## ASSOCIATED CONTENT

### Supporting Information

The Supporting Information is available free of charge on the ACS Publications website at DOI: [10.1021/acs.energyfuels.9b00057](https://doi.org/10.1021/acs.energyfuels.9b00057).

Determination of the dispersion coefficient  $D$ , derivation of the advection–dispersion–adsorption equations, and high-resolution SEM images (PDF)

## AUTHOR INFORMATION

### Corresponding Author

\*E-mail: [zsun@utexas.edu](mailto:zsun@utexas.edu).

### ORCID

Qi Liu: [0000-0001-5245-1311](https://orcid.org/0000-0001-5245-1311)

### Notes

The authors declare no competing financial interest.

## ACKNOWLEDGMENTS

Support for this research was provided by the KAUST endowment. G. E. Abelskamp edited the manuscript. Datasets presented as part of this study are available from authors.

## REFERENCES

- (1) Zhang, W.-x. Nanoscale iron particles for environmental remediation: an overview. *J. Nanopart. Res.* **2003**, *5*, 323–332, DOI: [10.1023/A:1025520116015](https://doi.org/10.1023/A:1025520116015).
- (2) Cundy, A. B.; Hopkinson, L.; Whitby, R. L. D. Use of iron-based technologies in contaminated land and groundwater remediation: a review. *Sci. Total Environ.* **2008**, *400*, 42–51.

- (3) Khin, M. M.; Nair, A. S.; Babu, V. J.; Murugan, R.; Ramakrishna, S. A review on nanomaterials for environmental remediation. *Energy Environ. Sci.* **2012**, *5*, 8075–8109.
- (4) Fu, F.; Dionysiou, D. D.; Liu, H. The use of zero-valent iron for groundwater remediation and wastewater treatment: a review. *J. Hazard Mater.* **2014**, *267*, 194–205.
- (5) Karimi, A.; Fakhroueian, Z.; Bahramian, A.; Pour Khiabani, N.; Darabad, J. B.; Azin, R.; Arya, S. Wettability alteration in carbonates using zirconium oxide nanofluids: EOR implications. *Energy Fuels* **2012**, *26*, 1028–1036.
- (6) Monfared, A. D.; Ghazanfari, M. H.; Jamialahmadi, M.; Helalizadeh, A. Potential Application of Silica Nanoparticles for Wettability Alteration of Oil-Wet Calcite: A Mechanistic Study. *Energy Fuels* **2016**, *30*, 3947–3961.
- (7) Al-Anssari, S.; Barifcani, A.; Wang, S.; Maxim, L.; Iglauer, S. Wettability alteration of oil-wet carbonate by silica nanofluid. *J. Colloid Interface Sci.* **2016**, *461*, 435–442.
- (8) Hendraningrat, L.; Li, S.; Torsæter, O. A coreflood investigation of nanofluid enhanced oil recovery. *J. Pet. Sci. Eng.* **2013**, *111*, 128–138.
- (9) Mohajeri, M.; Hemmati, M.; Shekarabi, A. S. An experimental study on using a nanosurfactant in an EOR process of heavy oil in a fractured micromodel. *J. Pet. Sci. Eng.* **2015**, *126*, 162–173.
- (10) Wasan, D. T.; Nikolov, A. D. Spreading of nanofluids on solids. *Nature* **2003**, *423*, 156.
- (11) Nikolov, A.; Zhang, H. The dynamics of capillary-driven two-phase flow: The role of nanofluid structural forces. *J. Colloid Interface Sci.* **2015**, *449*, 92–101.
- (12) Luo, D.; Wang, F.; Zhu, J.; Cao, F.; Liu, Y.; Li, X.; Ren, Z. Nanofluid of graphene-based amphiphilic Janus nanosheets for tertiary or enhanced oil recovery: High performance at low concentration. *Proc. Natl. Acad. Sci. U.S.A.* **2016**, *113*, 7711.
- (13) Suleimanov, B. A.; Ismailov, F. S.; Veliyev, E. F. Nanofluid for enhanced oil recovery. *J. Pet. Sci. Eng.* **2011**, *78*, 431–437.
- (14) Wei, B.; Li, Q.; Jin, F.; Li, H.; Wang, C. The potential of a novel nanofluid in enhancing oil recovery. *Energy Fuels* **2016**, *30*, 2882–2891.
- (15) McDowell-Boyer, L. M.; Hunt, J. R.; Sitar, N. Particle transport through porous media. *Water Resour. Res.* **1986**, *22*, 1901–1921.
- (16) Lecoanet, H. F.; Bottero, J.-Y.; Wiesner, M. R. Laboratory assessment of the mobility of nanomaterials in porous media. *Environ. Sci. Technol.* **2004**, *38*, 5164–5169.
- (17) Dunphy Guzman, K. A.; Finnegan, M. P.; Banfield, J. F. Influence of surface potential on aggregation and transport of titania nanoparticles. *Environ. Sci. Technol.* **2006**, *40*, 7688–7693.
- (18) Lønøy, A. Making sense of carbonate pore systems. *AAPG Bull.* **2006**, *90*, 1381–1405.
- (19) Hosseini, S. M.; Tosco, T. Transport and retention of high concentrated nano-Fe/Cu particles through highly flow-rated packed sand column. *Water Res.* **2013**, *47*, 326–338.
- (20) Ben-Moshe, T.; Dror, I.; Berkowitz, B. Transport of metal oxide nanoparticles in saturated porous media. *Chemosphere* **2010**, *81*, 387–393.
- (21) Chowdhury, I.; Hong, Y.; Honda, R. J.; Walker, S. L. Mechanisms of TiO<sub>2</sub> nanoparticle transport in porous media: Role of solution chemistry, nanoparticle concentration, and flowrate. *J. Colloid Interface Sci.* **2011**, *360*, 548–555.
- (22) He, F.; Zhang, M.; Qian, T.; Zhao, D. Transport of carboxymethyl cellulose stabilized iron nanoparticles in porous media: Column experiments and modeling. *J. Colloid Interface Sci.* **2009**, *334*, 96–102.
- (23) Sagee, O.; Dror, I.; Berkowitz, B. Transport of silver nanoparticles (AgNPs) in soil. *Chemosphere* **2012**, *88*, 670–675.
- (24) Kasel, D.; Bradford, S. A.; Šimůnek, J.; Heggen, M.; Vereecken, H.; Klumpp, E. Transport and retention of multi-walled carbon nanotubes in saturated porous media: Effects of input concentration and grain size. *Water Res.* **2013**, *47*, 933–944.
- (25) Lecoanet, H. F.; Wiesner, M. R. Velocity effects on fullerene and oxide nanoparticle deposition in porous media. *Environ. Sci. Technol.* **2004**, *38*, 4377–4382.
- (26) Yu, J.; An, C.; Mo, D.; Liu, N.; Lee, R. L. Study of adsorption and transportation behavior of nanoparticles in three different porous media. *SPE Improved Oil Recovery Symposium*; Society of Petroleum Engineers, 2012.
- (27) Zhang, T.; Murphy, M. J.; Yu, H.; Bagaria, H. G.; Yoon, K. Y.; Nielson, B. M.; Bielawski, C. W.; Johnston, K. P.; Huh, C.; Bryant, S. L. Investigation of nanoparticle adsorption during transport in porous media. *SPE J.* **2015**, *20*, 667–677.
- (28) Petosa, A. R.; Jaisi, D. P.; Quevedo, I. R.; Elimelech, M.; Tufenkji, N. Aggregation and deposition of engineered nanomaterials in aquatic environments: role of physicochemical interactions. *Environ. Sci. Technol.* **2010**, *44*, 6532–6549.
- (29) Wang, M.; Gao, B.; Tang, D. Review of key factors controlling engineered nanoparticle transport in porous media. *J. Hazard Mater.* **2016**, *318*, 233–246.
- (30) Fang, J.; Shan, X.-q.; Wen, B.; Huang, R.-x. Mobility of TX100 suspended multiwalled carbon nanotubes (MWCNTs) and the facilitated transport of phenanthrene in real soil columns. *Geoderma* **2013**, *207–208*, 1–7.
- (31) Schlumberger. *Carbonate Reservoirs: Meeting Unique Challenges to Maximize Recovery*, 2007.
- (32) Esfandyari Bayat, A.; Junin, R.; Samsuri, A.; Piroozian, A.; Hokmabadi, M. Impact of metal oxide nanoparticles on enhanced oil recovery from limestone media at several temperatures. *Energy Fuels* **2014**, *28*, 6255–6266.
- (33) Roustaei, A.; Bagherzadeh, H. Experimental investigation of SiO<sub>2</sub> nanoparticles on enhanced oil recovery of carbonate reservoirs. *J. Pet. Explor. Prod. Technol.* **2015**, *5*, 27–33.
- (34) Nazari Moghaddam, R.; Bahramian, A.; Fakhroueian, Z.; Karimi, A.; Arya, S. Comparative study of using nanoparticles for enhanced oil recovery: wettability alteration of carbonate rocks. *Energy Fuels* **2015**, *29*, 2111–2119.
- (35) Zhang, H.; Nikolov, A.; Wasan, D. Enhanced oil recovery (EOR) using nanoparticle dispersions: Underlying mechanism and imbibition experiments. *Energy Fuels* **2014**, *28*, 3002–3009.
- (36) Zhang, H.; Ramakrishnan, T. S.; Nikolov, A.; Wasan, D. Enhanced Oil Recovery Driven by Nanofilm Structural Disjoining Pressure: Flooding Experiments and Microvisualization. *Energy Fuels* **2016**, *30*, 2771–2779.
- (37) Monfared, A. D.; Ghazanfari, M. H.; Jamialahmadi, M.; Helalizadeh, A. Adsorption of silica nanoparticles onto calcite: Equilibrium, kinetic, thermodynamic and DLVO analysis. *Chem. Eng. J.* **2015**, *281*, 334–344.
- (38) Júnior, J. A. A.; Baldo, J. B. The behavior of zeta potential of silica suspensions. *New J. Glass Ceram.* **2014**, *4*, 29.
- (39) Melanson, J. E.; Baryla, N. E.; Lucy, C. A. Dynamic capillary coatings for electroosmotic flow control in capillary electrophoresis. *TrAC, Trends Anal. Chem.* **2001**, *20*, 365–374.
- (40) Tadros, T. F.; Lyklema, J. Adsorption of potential-determining ions at the silica-aqueous electrolyte interface and the role of some cations. *J. Electroanal. Chem. Interfacial Electrochem.* **1968**, *17*, 267–275.
- (41) Al Mahrouqi, D.; Vinogradov, J.; Jackson, M. D. Zeta potential of artificial and natural calcite in aqueous solution. *Adv. Colloid Interface Sci.* **2016**, *240*, 60.
- (42) Santamarina, J. C. Soil behavior at the microscale: particle forces. *Soil Behavior and Soft Ground Construction*, 2003; pp 25–56.
- (43) Bhattacharjee, S.; Elimelech, M. Surface element integration: a novel technique for evaluation of DLVO interaction between a particle and a flat plate. *J. Colloid Interface Sci.* **1997**, *193*, 273–285.
- (44) Adamczyk, Z. Particle adsorption and deposition: role of electrostatic interactions. *Adv. Colloid Interface Sci.* **2003**, *100–102*, 267–347.
- (45) Israelachvili, J. N. *Intermolecular and Surface Forces*; Academic press, 2011.

(46) Cameron, D. R.; Klute, A. Convective-dispersive solute transport with a combined equilibrium and kinetic adsorption model. *Water Resour. Res.* **1977**, *13*, 183–188.